



FULL PAPER

Open Access



Ionospheric irregularity behavior during the September 6–10, 2017 magnetic storm over Brazilian equatorial–low latitudes

Eurico R. de Paula^{1*}, Cesar B. A. de Oliveira², Ronald G. Caton³, Patricia M. Negreti¹, Inez S. Batista¹ , André R. F. Martinon¹, Acácio C. Neto⁴, Mangalathayil A. Abdu¹, João F. G. Monico⁵, Jonas Sousasantos² and Alison O. Moraes⁶ 

Abstract

The September 6–10, 2017 two-step magnetic storm was caused by an X9 solar flare followed by a CME. The SSC that occurred at 23:43 UT on day 06 when Sym-H reached about 50 nT, was due to a sudden increase in solar wind. The first step of the storm was caused by a B_z southward incursion on day 07. The magnetic index K_p reached 08, and the Sym-H magnetic index reached a minimum value of -146 nT on day 08 at 01:08 UT, ending the main phase. On day 07, the solar wind intensified once again and the auroral index AE reached 2500 nT. During the recovery phase of this first storm, there was another B_z southward incursion on day 08 at 13:56 UT when Sym-H reached -115 nT, and K_p reached a value of 08.33, marking the second step of the storm. In this work, the ionospheric irregularity over São Luís (02.5°S, 44.3°W, dip lat -04.67°) was studied using data from the VHF, Digisonde and GPS receivers. Electron density data from the satellite SWARM-A were also analyzed for those orbits close to São Luís, and they presented large fluctuations during the storm night of 07/08. To analyze the latitudinal effects of the storm on the plasma irregularities, GPS data from 6 Novatel receivers were used. The vertical plasma drifts during daytime hours were determined using magnetometer data and during the evening using ionogram data. Compared to the 'quiet' days of September 2017, the VHF and GPS S4 amplitude scintillation indices increased substantially during the night of 07/08 when there was a strong intensification in the vertical plasma drift due to a prompt penetration under shielding magnetospheric electric field of eastward polarity. On the other hand, on the night of 08/09 the ionospheric scintillation was completely inhibited due to the disturbance dynamo electric field of westward polarity associated with the first and second storms. The irregularity zonal drifts measured by a VHF receiver around 24 UT (21 LT) were eastward on the nights of 05/06 and 06/07; however, during the night of 07/08, it reversed to westward.

Keywords: Ionospheric irregularity, Ionospheric scintillation, Magnetic storm, Magnetospheric electric field penetration, Counter-electrojet, Plasma irregularity zonal velocity

Introduction

In the post-sunset equatorial ionosphere, the steep electron density gradient at the F region bottom side may lead to plasma irregularity development through the Rayleigh–Taylor instability process. In this process, the low-density plasma from lower heights is lifted up to

the F region topside leading to the generation of rarefied field-aligned structures called equatorial plasma bubbles (EPBs) with scale sizes of tens to hundreds of kilometers. The upward and field-aligned growth of the bubble is nonlinear and is accompanied by generation of secondary irregularities through cascading processes (Sultan 1996; Keskinen et al. 2003) resulting in the formation of centimeter-to-meter scale size irregularities. The EPBs normally drift eastward during pre-midnight hours during magnetically quiet periods. However, under magnetic

*Correspondence: eurico.paula@inpe.br

¹ Instituto Nacional de Pesquisas Espaciais, São José dos Campos, São Paulo 12.227-010, Brazil

Full list of author information is available at the end of the article

storm conditions, typically the EPBs drift reverses to westward. Such characteristics of the bubble zonal drift have been reported from the Indian sector by Engavale et al. (2005) and Bhattacharyya et al. (2002). Plasma bubbles drifting westward during magnetic storms were observed in the Brazilian sector by Abdu et al. (2003) and Santos et al. (2016). They pointed out that the thermospheric zonal wind perturbation, as well as the vertical Hall electric field mapped from the E region, could be the drivers for the westward drift. Huang and Roddy (2016) analyzed Communications/Navigation Outage Forecasting System (C/NOFS) satellite data from 2008 to 2014, and they pointed out that enhanced geomagnetic activities cause a westward plasma drift in the nighttime equatorial region through the effect of the DD process. Kakad et al. (2017) analyzed 3 near-similar storms, except their start time, with the same behavior on the Indian sector during April and September 2011. They observed that the Disturbance Dynamo (DD) effects in the zonal irregularity drifts seen in low-latitude *F* region around midnight became more pronounced as ΔT decreases, where ΔT is the time difference between the Storm Sudden Commencement (SSC) and the local sunset time.

The main parameter responsible for the plasma bubble irregularity generation and evolution is the vertical plasma drift during the evening prereversal hours (Fejer et al. 1999). The bubble irregularity growth is regulated also by the magnetic field line integrated conductivity which is controlled by transequatorial/meridional winds and the planetary/gravity waves that propagate upward to the ionospheric *F* region (Abdu and Kherani 2011).

The smaller-scale structures that develop in the walls of the bubbles may contribute to scintillation in the phase and amplitude of radio signals propagating through them. The ionospheric scintillations present large degree of variability on a day-to-day basis with local time, season, solar activity (Muella et al. 2017), magnetic storm and sudden stratospheric warming—SSW events (de Paula et al. 2015). At the Brazilian longitudes, characterized by large westward magnetic declination angle, the post-sunset scintillations occur mainly during the period extending from September to March/April. The scintillation occurrence pattern can be modified drastically during magnetic storms when magnetospheric electric fields may promptly penetrate (PPEF) to equatorial latitudes in the form of undershielding/overshielding electric fields or as disturbance dynamo electric fields (DDEF) (Fejer and Scherliess 1997; Scherliess and Fejer 1997). Depending upon local time, these electric fields can be directed westward or eastward. The DDEF is normally westward during the day and evening hours and mostly eastward during night. Undershielding/overshielding PPEFs are

directed eastward/westward during the day and evening hours, and westward/eastward during the night. A magnetospheric eastward electric penetrating during the evening prereversal hours can contribute to large upward vertical plasma drifts, leading to the generation of plasma irregularities and subsequent scintillation effects, even during a season non-occurrence of scintillation (Abdu et al. 2003, 2008; de Paula et al. 2004). On the other hand, a westward DDEF can inhibit the evening prereversal drift and consequently the irregularities generation. Abdu et al. (2009) presented a case of overshielding penetration electric field (PEF) of westward polarity that caused suppression of the prereversal vertical drift enhancement (PRE) and non-occurrence of the ionospheric irregularities. Their results were evaluated using a collisional interchange instability growth rate model. Also, Nayak et al. (2017) observed a case of westward PPEF during the March 17, 2015 St. Patrick super storm, when scintillation suppression was observed at the longitudinal sector of Taiwan, while scintillations were observed in the Indian sector. Similar results over Indian sector for the same storm were reported by Carter et al. (2016). It is now well known that scintillation suppression during post-sunset time can occur over most of the longitudinal sectors.

According to Aarons (1991), the time when maximum Dst decrease occurs, or when PPEF penetrates to low latitudes, may determine whether or not the plasma irregularity generation will follow. He classified the maximum Dst occurrence time into 3 categories: (1) 10:00–16:00 LT, (2) 00:00–06:00 LT and (3) 18:00–22:00 LT, being the first category typical of post-sunset irregularities inhibition, the second one favorable for post-midnight occurrence and the last one favorable for post-sunset generation. de Paula et al. (2004) analyzed data for the April 10–13, 2001 magnetic storm and observed the occurrence of large plumes over the São Luís VHF backscatter radar during the storm main phase (Aarons class 3 event) on day 11 with the presence of simultaneous strong scintillations, which were detected by GPS receivers. No scintillation was observed on the previous and posterior days of this storm, which is the expected scintillation behavior for the month of April over Brazil (de Paula et al. 2007). Li et al. (2008) analyzed the effect of 3 magnetic storms on GPS ionospheric scintillation at Sanya (18.31°N, 109.5°E) during 2005, and they also observed that during 2 storms with Dst decrease larger than -100 nT, the storm triggered scintillation during its non-occurrence season (May and August). No scintillation was observed during a third storm that also occurred during May 2005. However, Defense Meteorological Satellite Program (DMSP) satellite data detected the presence of large

structure over a different longitudinal sector (191°E). Li et al. (2008) pointed out that one important parameter to determine the magnetospheric electric field penetration to low latitude is the maximum $dDst/dt$ in the occurrence time, which supports the work of Martinis et al. (2005). Kakad et al. (2012) pointed out that the power spectral characteristics of the ionospheric irregularities during magnetic storms could be different from those at quiet time, which suggest the difference in their structuring of ESF irregularities.

The main objective of the present work is to analyze the ionospheric irregularities behavior during the magnetic storm of September 6–10, 2017. This storm was caused by an X9 solar flare followed by a coronal mass ejection (CME). Three other less intense flares followed the X9 event. To characterize the magnetic storm, Fig. 1 presents, for this period, the solar wind velocity V_{sw} , the north–south interplanetary magnetic field (IMF) component B_z , the interplanetary east–west electric field E_y , the magnetic indices K_p , Sym-H, and the auroral magnetic index AE. The vertical dashed red lines represent the 2 storm sudden commencements (SSC), the first one at 23:43 UT on day 06 and the other at 23:00 UT on day 07 (<http://www.obsebre.es/en/rapid>). The LT axis for the geographic longitude of 45°W is plotted at the upper panel (LT = UT-03). The solar wind speed increased from 400 to about 600 km/s around 24 UT of day 06 and to about 800 km/s on the following night of 07/08. The IMF B_z component presented a first southward turning at 20:40 UT on day 07 reaching about -10 nT and remaining at this level for 2 h when the AE index reached about 1000 nT. Following an intense B_z southward incursion of -31.21 nT was observed at 23:31 UT (20:31 LT) and turned to north at 02:00 UT on day 08. After this, B_z negative incursion fast and less intense north–south B_z fluctuations were observed. On day, 08 Sym-H reached a minimum value of -146 nT at 01:08 UT during the initiation of the first storm recovery phase, and K_p reached 8 from 00 to 03 UT. During the recovery phase of this first storm, there was another B_z southward excursion of -17.46 nT at 11:55 UT on day 08 for about 4 h, when Sym-H reached -115 nT at 13:56 UT and K_p reached 8.33 around noon. The interplanetary east–west E_y electric field reached peak values of 21.21 mV/m at 23:49 UT of day 7 and 13 mV/m at 11:58 UT on day 08, both being eastward and due to undershielding conditions. The auroral index AE increased to more than 2000 nT on days 07 and 08 during the main and recovery phase of the first magnetic storm of 07/08, respectively.

All the parameters in Fig. 1 have 1-min resolution, except K_p . When V_{sw} , B_z and E_y 1-min data for days 09 and 10 were not available at the site: <https://omniweb.gsfc.nasa.gov>, hourly values from this site were used.

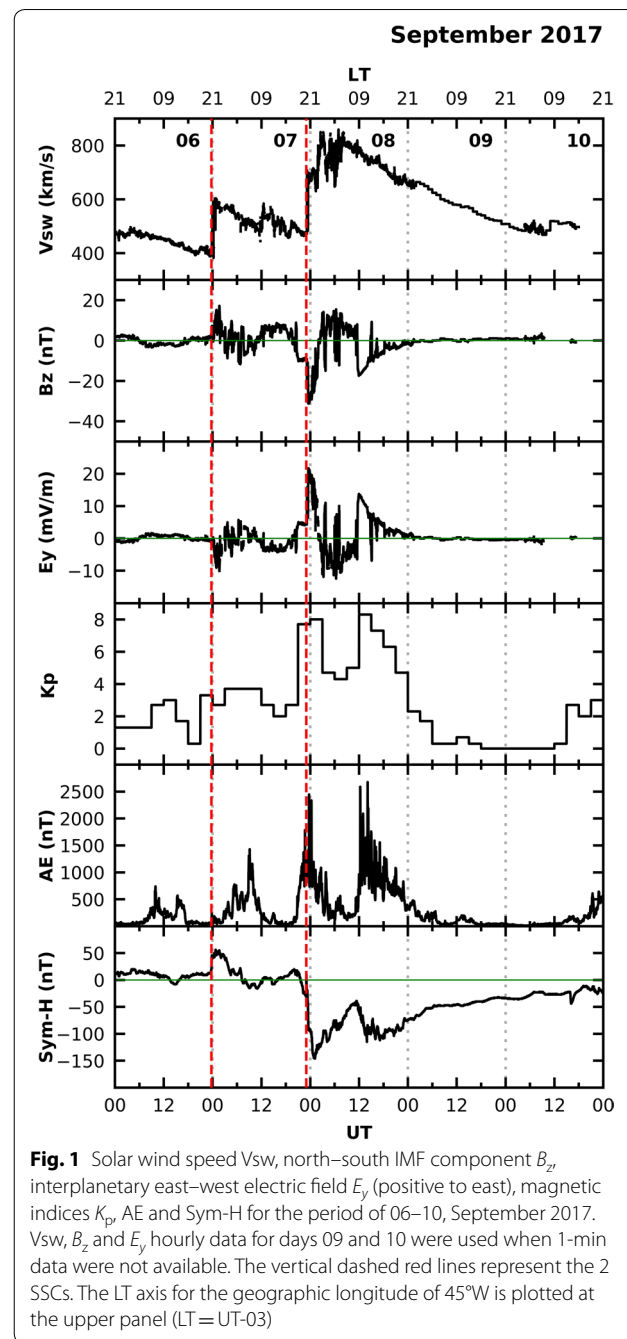


Fig. 1 Solar wind speed V_{sw} , north–south IMF component B_z , interplanetary east–west electric field E_y (positive to east), magnetic indices K_p , AE and Sym-H for the period of 06–10, September 2017. V_{sw} , B_z and E_y hourly data for days 09 and 10 were used when 1-min data were not available. The vertical dashed red lines represent the 2 SSCs. The LT axis for the geographic longitude of 45°W is plotted at the upper panel (LT = UT-03)

Methodology and data

To study the plasma irregularity behavior and to point out the possible physical mechanisms responsible for the irregularities generation or inhibition during this storm, the data obtained from the GPS and 240 MHz VHF receivers, and from the Digisonde at São Luís (02.5°S, 44.3°W, dip lat -04.67°). The data from a network of GPS receivers distributed in a latitudinal range of 4.7° – 20.9° S were also employed. To calculate the daytime vertical

plasma drifts, the data from the magnetometers at Belém (1.5°S, 48.5°W, dip lat -1.12°) and Petrolina (09.4°S, 40.5°W, dip lat -13.45°) were used. The SWARM-A satellite electron density data measured during its passages over the Brazilian longitudes close to São Luís for the quiet day 03, and disturbed days 07 and 08 of September 2017, were also analyzed. A brief description of these ionospheric and magnetic measurements and data processing methodologies are provided below.

A software-defined receiver (SDR)-based scintillation data recorder provided by Air Force Research Laboratory (AFRL) and managed through Boston College collects VHF amplitude data from São Luís, Brazil at ~ 240 MHz from a geostationary satellite. In addition to the raw amplitude signatures, archived at 50 Hz, the statistical parameters for the S4 and decorrelation time are computed over 1-min intervals to characterize the scintillation fading environment. A spaced-antenna configuration with high-gain yagis separated by ~ 100 m in the magnetic zonal direction is used to measure the ionospheric zonal drift velocity through a cross-correlation of the raw amplitude (Groves et al. 1997). A colocated GPS receiver provides specifications of the local scintillation environment at L-band frequency. The VHF scintillation data recorded from this location are representative of the ionospheric environment to the east of São Luís from a link at $\sim 64^\circ$ elevation. It is important to note that the amplitude scintillations on VHF frequency are sensitive to the first Fresnel zone ($\sqrt{2\lambda Z}$), which is approximately 930 m. Here λ is the wavelength of the radio signal, and Z is the height of irregularity layer assumed to be 350 km. The duration of scintillation at VHF can be many hours more than that at L-band frequency which is sensitive to scale sizes of approximately 400 m.

A Septentrio PolaRx5 GPS receiver, from the CIGALA/CALIBRA network (<http://is-cigala-calibra.fct.unesp.br/is/>), provided parameters of amplitude and phase of the L1, L2C and L5 frequencies at a rate of 50 Hz and 1-min averages of the S4 index and σ_ϕ for São Luís. Phase scintillation σ_ϕ is not considered in this work. Only data for satellite elevations higher than 30° were considered in the analysis to avoid multipath and weak signal-to-noise ratio. To complement São Luís data, GPS data from the Novatel 4004B receivers from Low-Latitude Ionospheric Sensor Network (LISN) consisting of the sites shown in Fig. 2 were also used. Their geographic coordinates and dip latitudes are presented in Table 1.

As the vertical plasma drift is an important parameter for the plasma irregularity generation (Fejer et al. 1999), this parameter was determined by two methodologies. The first one was by using the true height data from the Digisonde at four fixed frequencies (4, 5, 6 and 7 MHz) around the vertical drift prereversal hours (21–24 UT)

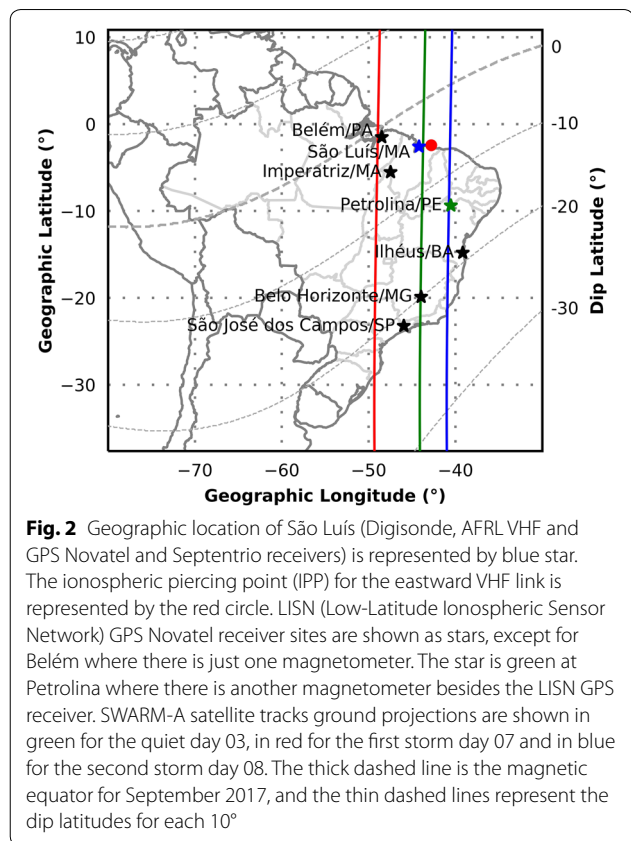


Fig. 2 Geographic location of São Luís (Digisonde, AFRL VHF and GPS Novatel and Septentrio receivers) is represented by blue star. The ionospheric piercing point (IPP) for the eastward VHF link is represented by the red circle. LISN (Low-Latitude Ionospheric Sensor Network) GPS Novatel receiver sites are shown as stars, except for Belém where there is just one magnetometer. The star is green at Petrolina where there is another magnetometer besides the LISN GPS receiver. SWARM-A satellite tracks ground projections are shown in green for the quiet day 03, in red for the first storm day 07 and in blue for the second storm day 08. The thick dashed line is the magnetic equator for September 2017, and the thin dashed lines represent the dip latitudes for each 10°

when the ionosphere is lifted up to higher altitudes. The vertical plasma drifts were calculated as $\Delta h/\Delta t$ (Bittencourt and Abdu 1981), in which Δt is the time resolution between two ionograms, equal to 10 min. The average vertical drift from these four frequencies is then determined. The second methodology, during daytime hours, uses data from a pair of magnetometers, one under the electrojet (Belém) and the other outside the electrojet (Petrolina), once the zonal electric field that drives the vertical drift is related to the equatorial electrojet strength. According to Anderson et al. (2002, 2004), the daytime vertical plasma drifts V_d were calculated using the following equation:

$$V_d = 12.26 - 0.0454F10.7 + 0.1892\Delta H + 0.00028\Delta H^2 - 0.00000022\Delta H^3 \quad (1)$$

[with an RMS error of about 3.36 m/s for the multiple regression method (Anderson et al. 2004)], where $\Delta H = H_{\text{Belém}} - H_{\text{Petrolina}}$ is the 1 min difference between the geomagnetic field horizontal component variation at Belém ($H_{\text{Belém}}$) and at Petrolina ($H_{\text{Petrolina}}$) and represents the electrojet intensity. The average values around midnight of the horizontal component H of the geomagnetic field are computed from measurements for the entire

Table 1 Geographic coordinates and dip latitudes of the GPS receivers

Station	Latitude	Longitude	Dip latitude
São Luís	02.5°S	44.3°W	04.7°S
Imperatriz	05.5°S	47.4°W	05.5°S
Petrolina	09.4°S	40.5°W	13.5°S
Ilhéus	14.8°S	39.0°W	19.1°S
Belo Horizonte	19.8°S	43.9°W	19.9°S
São José dos Campos	23.2°S	45.9°W	20.9°S

period and subtracted from $H_{\text{Belém}}$ and from $H_{\text{Petrolina}}$ in order to extract the background field, remaining only the electrojet strength during daytime. The Belém and Petrolina magnetometer data were obtained from the SAMBA-AMBER magnetometer data center (<http://magnetometers.bc.edu/index.php/amber2>). $F_{10.7}$ is the solar flux index, and the values of $F_{10.7}$ were 134.9, 130.4, 118.5, 108.7 and 101.6 units for the days 06, 07, 08, 09 and 10, respectively. These solar flux values were obtained from <https://omniweb.gsfc.nasa.gov>.

In this work, the zonal bubble horizontal velocity is determined also using the São Luís Lowell Digisonde that has 4 receiving antennas, forming an equilateral triangle with 60 m of spacing between them and one antenna located at the center of the triangle. Using this procedure and calculating the Doppler shift of the antenna signals, it is possible to infer the vertical, north–south and the east–west (zonal) velocity components of the ionospheric irregularities/plasma bubbles (Reinisch et al. 1998). Besides, the two methodologies described above, the ionospheric bubble zonal drift velocity was inferred also by constructing a keogram from the GPS total electron content (TEC) data for a given geographic latitude. The methodology to obtain the keogram is by mounting a temporal sequence of 2D TEC maps for the selected day, resulting in a 3D TEC map (latitude, longitude and time). Following, one latitudinal cut for a time sequence is done for the selected geographic latitude of 10°S. With this procedure, it is possible to follow the bubble zonal displacements in the spatial domain.

The in situ electron density measured by the Langmuir probe onboard the European Space Agency (ESA) SWARM-A satellite was also used for the days 03 (quiet), 07 (storm) and 08 (storm). These three selected SWARM-A orbit projections over ground close to São Luís from about 00:30 to 01:40 UT (21:30–22:40 LT) were used since this time interval is conducive to formation of plasma irregularities. The circular orbit of this satellite is at about 460 km of altitude and it has

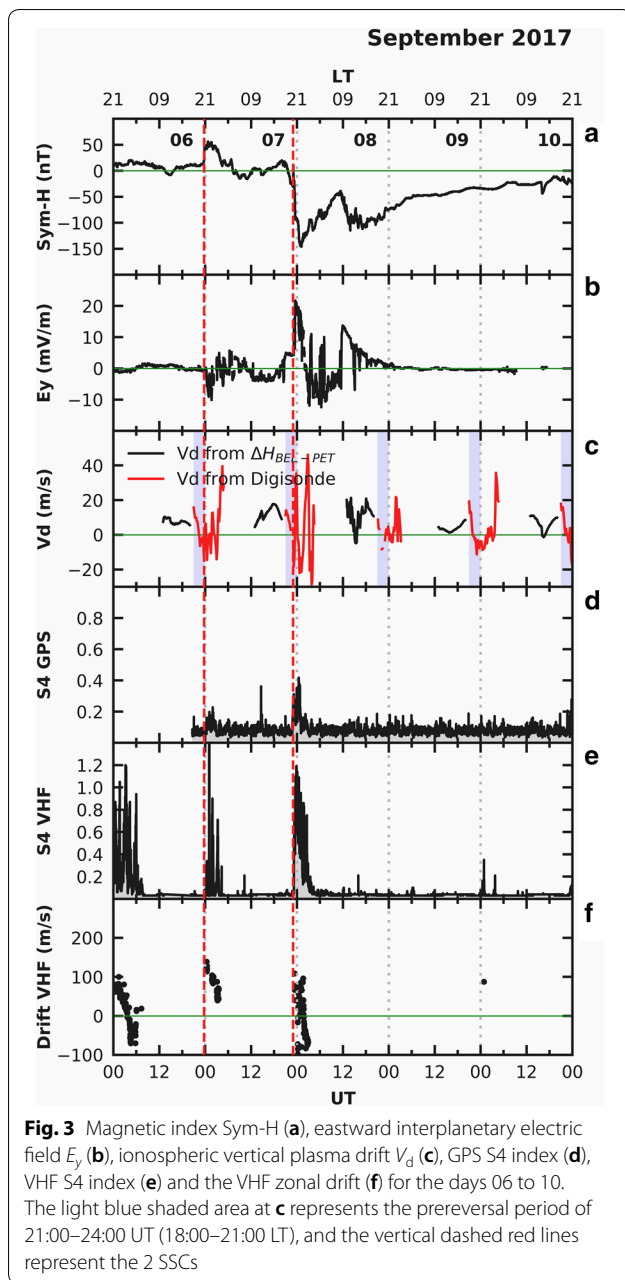
a very large inclination (87.5°), so during its equatorial crossing has small time variation across all latitudes for each pass over Brazil. These data were obtained from the site <http://earth.esa.int/swarm>.

Figure 2 shows the geographic location of São Luís where the Lowell University Digisonde, the AFRL VHF receiver and the GPS receivers are installed. Also shown in this figure is the IPP (Ionospheric Piercing Point) at 350 km of altitude for the eastward VHF link. The SWARM-A satellite tracks ground projections are shown in green for the quiet day 03, in red for the first storm day 07 and in blue for the second storm day 08. The dashed line is the magnetic equator for September 2017 inferred from IGRF (International Geomagnetic Reference Field) in the site <http://wdc.kugi.kyoto-u.ac.jp/igrf/index.html>. Additionally, the data from the LISN GPS Novatel receivers (<http://lisn.igp.gob.pe/>), shown in Fig. 2, were used to complement the São Luís data. Magnetometer sites, Belém (black star) and Petrolina (green star), are also shown at this figure.

Results and discussions

In this section, the data from Digisonde, VHF and GPS receivers and SWARM-A satellite during the 06–10, September magnetic storm are presented. The physical mechanisms responsible for the counter-electrojet observed during daytime hours of day 08 and for the scintillation generation on the night 07/09 and inhibition on the night 08/09 are pointed out. To analyze the effect of this storm in the VHF and GPS ionospheric scintillation, Fig. 3 presents the magnetic index Sym-H (panel a), the eastward interplanetary electric field E_y (panel b), the nighttime ionospheric vertical plasma drift V_d inferred from Digisonde data in red and the daytime using magnetometers data in black (panel c), the Septentrio GPS S4 index (panel d), the VHF S4 index (panel e) and the VHF zonal drift (panel f) for the days 06–10 of September 2017 storm period. The dashed vertical red lines indicate the SSCs, the first one at 23:43 UT on day 06 and the second one at 23:00 UT on day 07. The light blue shaded areas in panel c represent the prereversal period in vertical drift (21–24 UT). The V_d , the S4 indices and the VHF zonal drifts were measured at São Luís. All these parameters are plotted with 1 min resolution, except V_d that is for each 10 min. As explained in Fig. 1 hourly values of E_y were used when there are no 1-min data for this parameter.

Figure 3b shows a strong undershielding eastward interplanetary electric field E_y of 21.21 mV/m at 23:49 UT on day 07, simultaneously with the first B_z southward incursion of larger intensity (see Fig. 1), that penetrated to the equatorial ionosphere. During this electric field penetration event, the upward vertical plasma drift



inferred from Digisonde data reached about 38 m/s around 23:50 UT on day 07. According to Abdu et al. (2018), rapid intensification of the AE index under the B_z south condition near sunset is a clear indicator of a PPEF of eastward polarity that can cause a rapid F layer uplift, with correspondingly larger PRE vertical drift. On the day 07, eastward PPEF penetration occurred at 23:49 UT (20:49 LT), and as explained above, it caused a large vertical plasma drift, which contributed to the spread F (SF) development during this night. Similar behavior was observed during the strong event of October 2013 (Abdu

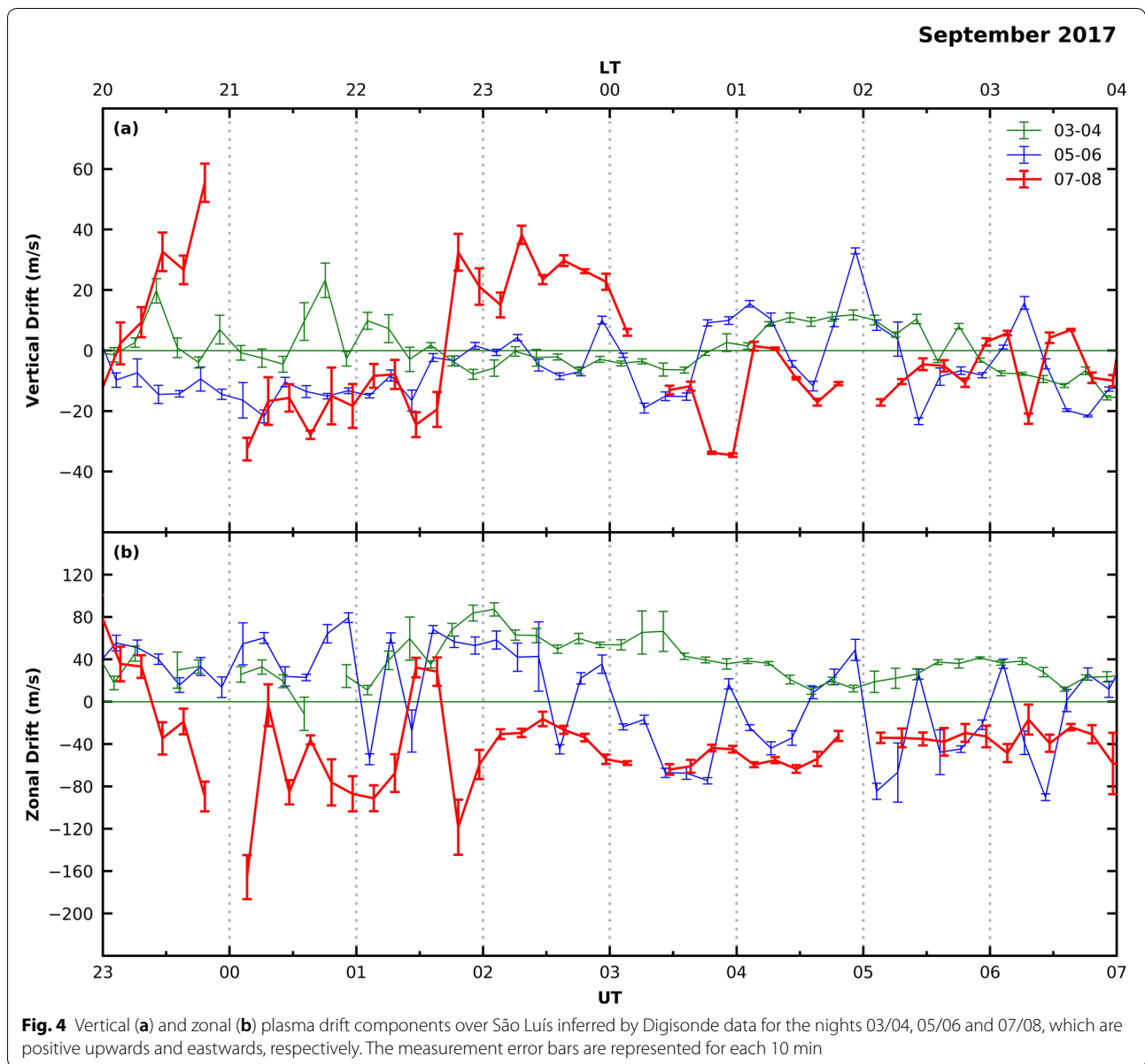
et al. 2008) and April 2002 (de Paula et al. 2004). All these eastward interplanetary electric field penetration events occurred during equinox and summer solstice over Brazilian longitude sector.

It should be noted that the Digisonde is operated at a temporal resolution of 10 min, and therefore, some uncertainties in time should be expected in the calculated vertical drifts. The large vertical drift of 38 m/s during the night 07/08 at about 23:50 UT was much higher than the vertical drifts observed during the other pre- (about 15 m/s) and post-storm (about 20 m/s) nights as presented in Fig. 3c. The large value of the prereversal drift velocity peak provided favorable conditions for the generation of plasma irregularities. Figure 3d and e shows that the GPS and VHF S4 indices are larger and have longer lasting duration on the night of the first storm main phase compared to the other nights of the 06–10 period, which is in agreement with the results obtained during the St. Patrick storm of 17 of March 2015 in the Indian sector (Kakad et al. 2016). One subsequent upward vertical plasma drift that attained a peak of about 40 m/s at 03 UT on day 08 (Fig. 3c) contributed to the intensified and long-lasting scintillation during the night of 07/08. A second E_y penetration of about 13 mV/m (Fig. 3b) occurred at 11:58 UT on day 08, causing a large fluctuation in the daytime vertical drift (Fig. 3c). This daytime event will be discussed in more detail later.

Ionospheric irregularity zonal drifts

Figure 3f presents zonal drifts calculated using data from spaced receivers monitoring VHF signals from a geostationary satellite. On the nights of 05/06 and 06/07, the zonal velocities around midnight were eastward and about 72.5 m/s and 125 m/s, respectively, and decreased with time. However, on the night of 07/08 the zonal velocity reversed to the west at 01:44 UT (22:44 LT) reaching a value of about -80 m/s around 02:53 UT on day 08. The bubble zonal drift reversal to the west on the storm night 07/08 was earlier than that on the night of 05/06 when the reversal occurred at 03:50 UT, characterizing a westward velocity before local midnight under the effect of the storm. On the night 06/07, the VHF zonal drift was more eastward than on the other nights; however, there were no VHF data enough (weaker scintillation) to reach inversion time.

As stated previously, another methodology to infer the zonal drifts is by using the Digisonde data. In the following, some results of this methodology will be presented. To complement zonal drift data, simultaneous vertical drift obtained by the Digisonde data is also presented. Figure 4 presents the ionospheric vertical (a) and zonal (b) plasma drifts inferred from the São Luís Digisonde data for the storm night 07/08 (red lines) and for the



magnetically quiet nights 03/04 (green) and 05/06 (blue). The measurement error bars are plotted at each 10 min that is the Digisonde temporal resolution. The upper panel shows an increase with time of the vertical drift on the night 07/08 increasing from -10 to about 55 m/s, in about 40 min. As discussed previously this uplift of the F layer to considerably higher altitudes, when compared to the nights 03/04 (green line) and 05/06 (blue line), is favorable to irregularity generation. Figure 4b shows that the zonal plasma drift reverts from east to west during the night 07/08 (red line) at 23:22 UT and maintains westward up to rest of this night, except during a short-lived eastward peak at 01:20 UT on day 08. This westward reversion time during the storm night 07/08 was earlier

than during the quiet nights 03/04 and 05/06 shown in the figure. On 05/06 (blue line), the zonal drift velocity remained mainly eastward until about 03:05 UT, and on 03/04 (green line), the zonal drift velocity was eastward during all the period. Abdu et al. (2003) and Santos et al. (2016) considered the perturbation in the zonal wind and the mapping of the E region electric field as the drivers for the westward drifts during magnetic storms, while Huang and Roddy (2016) pointed out that the zonal plasma drift reversion from east to west can be due to DD effects.

As explained previously, a third alternative methodology to infer the irregularity zonal velocity is by using keograms prepared from the GPS TEC data. In this work, a

keogram was obtained for the geographic latitude of 10°S. The aim of presenting this methodology is to compare zonal velocities obtained from this method (which considers a macro-observation) with the velocities inferred from Digisonde and from spaced VHF receivers. Figure 5 shows the zonal bubble drift velocity for the night 07/08 presented in the form of a keogram. In this figure, it can be identified that a TEC depletion was initiated a little bit before 00:00 UT as shown by the white dotted line. The structure inclination presented in this keogram represents a westward average zonal velocity of about 49 m/s during the bubble existence, which is in reasonable agreement with the zonal drift inferred by the Digisonde data presented in Fig. 4b and VHF zonal drifts presented in Fig. 3f.

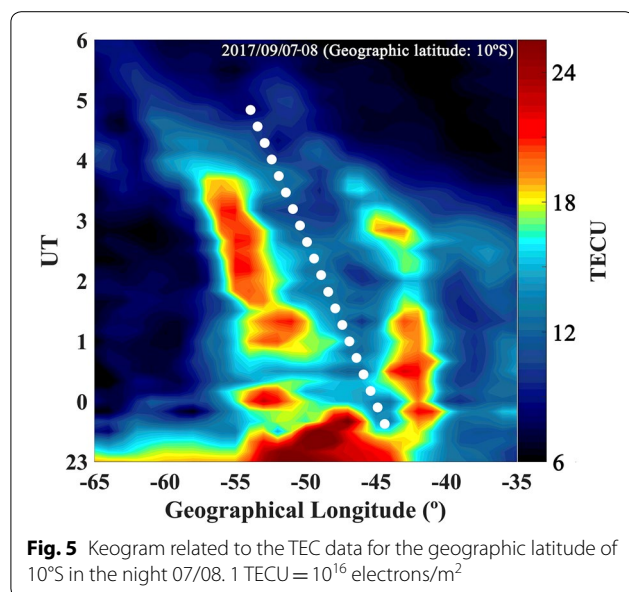
Digisonde F layer peak densities, $h'F$ and true heights

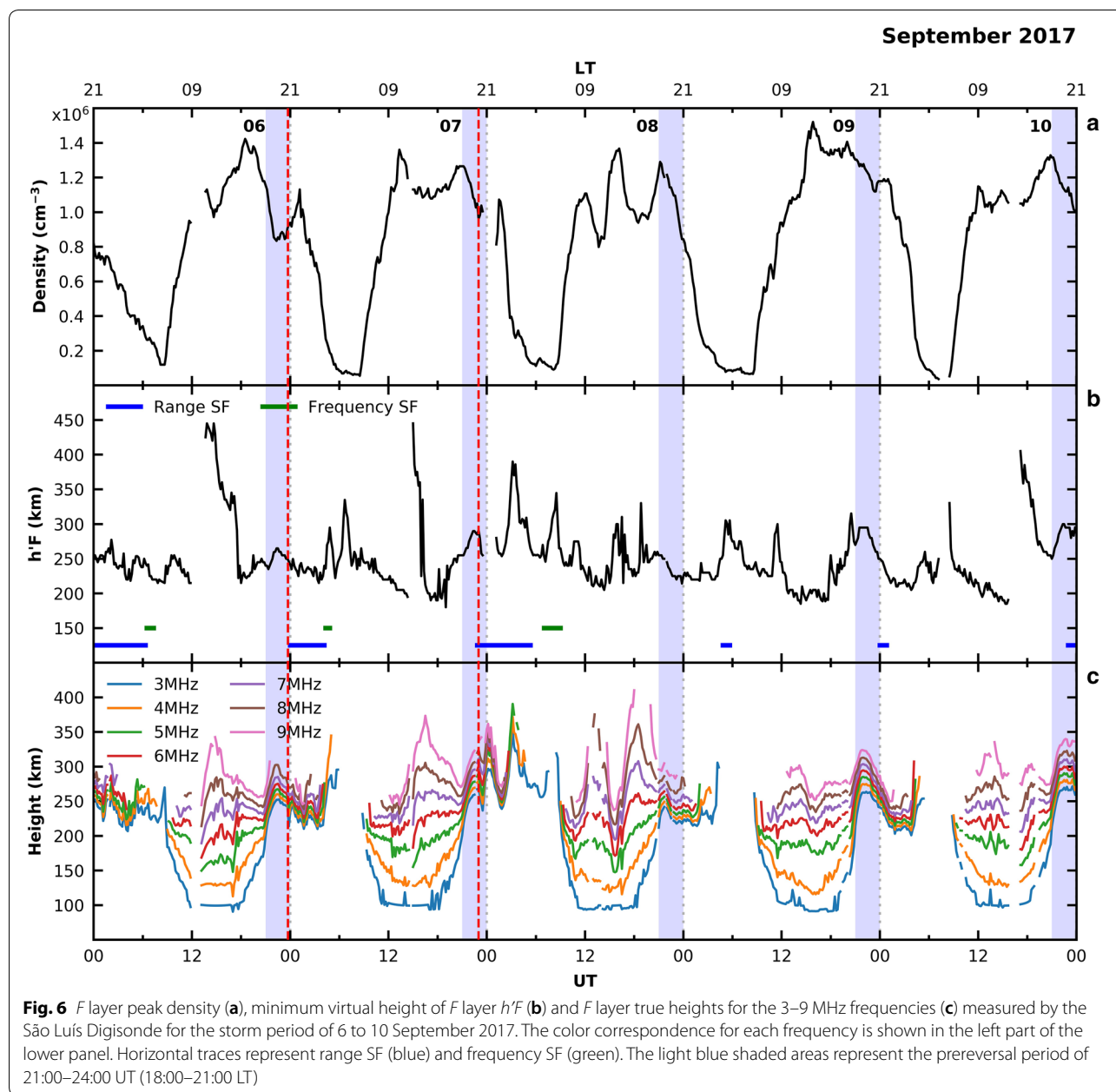
To provide more information about F layer peak density, minimum virtual height and true heights during this storm, Fig. 6a shows the F layer peak density deduced from foF2 (maximum frequency of F layer ordinary trace), panel b, the minimum virtual height of F layer ($h'F$) and panel c the F layer true heights for the 3 to 9 MHz frequencies, measured by the Digisonde at São Luís. Panel b shows also the range (blue) and frequency (green) SF occurrence duration represented by horizontal bars. Long-lasting range spread F (more than 6 h) was observed on the storm night of 07/08, after an $h'F$ upward movement from 200 km at 18:00 UT to about 290 km at 22:40 UT on day 07. A frequency spread F occurred from 06:20 UT to 09:00 UT on day 08. The SF was inhibited on the night 08/09 following $h'F$ downward movement

from 22:00 UT to 24:00 UT on day 08. Only a very short-lived range SF was observed from 04:30 UT to 06:00 UT on day 09. Figure 6b shows that on days 06, 07 and 10 the $h'F$ parameter presented data gaps followed by large values, due to the total or partial absorption of the HF wave by the increased D region density due to the flare X-ray radiation. Large fluctuations on peak density and F layer height during daytime hours of day 08 are observed (Fig. 6c). Much higher F layer altitudes can be observed in Fig. 6c, around prereversal hours on the night 07/08 during the first storm recovery phase initiation, compared to the other nights. Prereversal peak in the vertical drift was observed on the days 06/07, 07/08, 09/10 and 10/11 (Fig. 6c), but it was completely inhibited on the night 08/09 September. In Fig. 6, light blue shaded areas represent the prereversal hours (21:00 UT–24:00 UT). At about 15 UT on day 08, a downward movement of the F layer height is evident, which appears to be signature of a counter-electrojet, when the zonal electric field reverses to westward. Simultaneously, an increase in the F layer peak electron density is observed.

Counter-electrojet, overshielding and disturbance dynamo effects

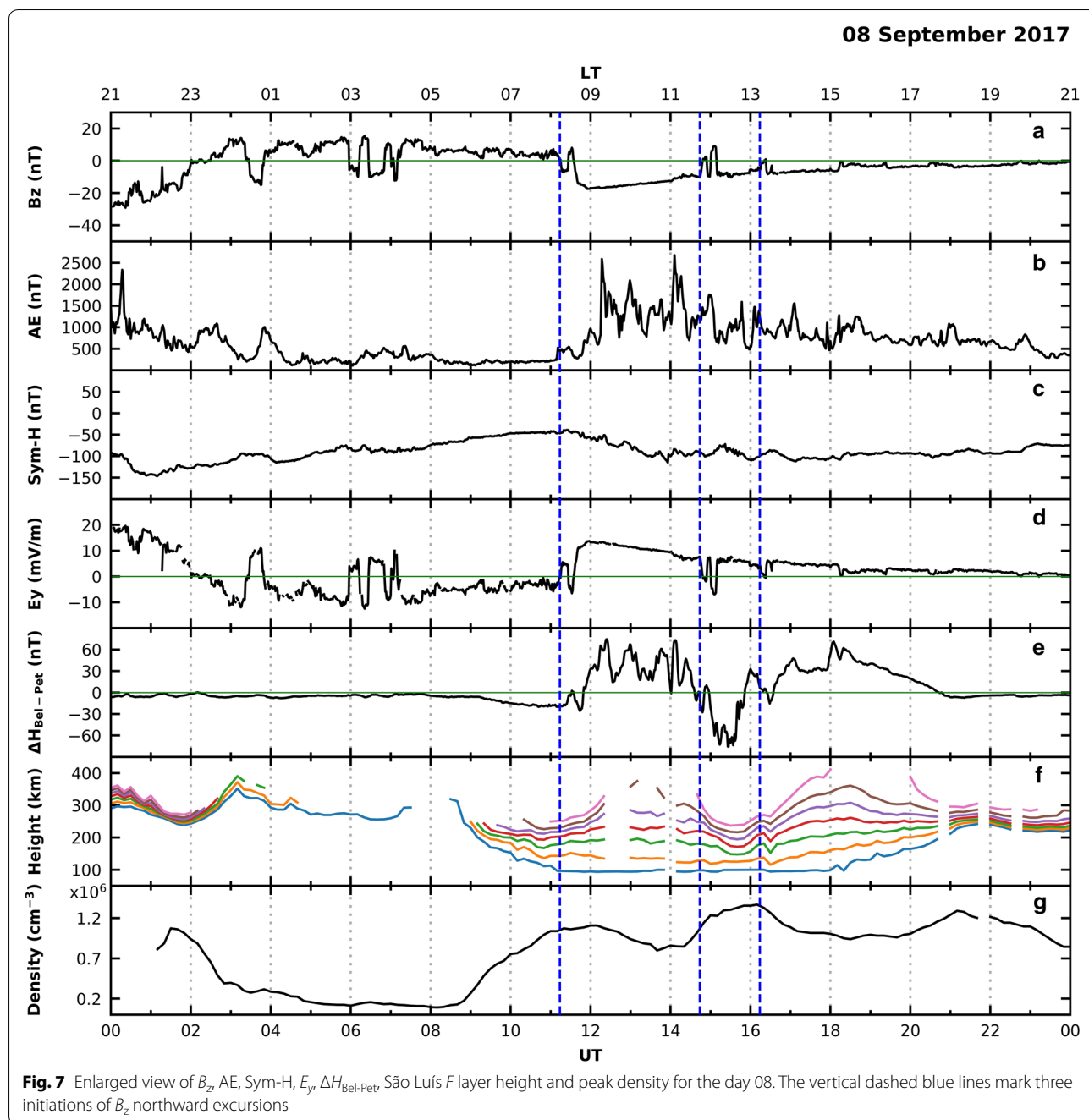
In order to discuss the event of a strong counter-electrojet (CEJ), we have plotted in Fig. 7 an extended view of the B_z , AE, Sym-H, E_y , $\Delta H_{\text{Bel-Pet}}$, São Luís F layer height and peak electron density for the day 08. The $\Delta H_{\text{Bel-Pet}}$ representing the electrojet intensity (panel e), presented much larger fluctuations and large negative deviation (counter-electrojet) on this day from about 14:40 to 16:10 UT, compared to the other days. During the recovery phase of the first magnetic storm (night of 07/08) and from about 11 UT up to 24 UT on day 08, there was a high-intensity and long-duration auroral activity. During this time interval, long-lasting B_z southward negative deviation and three short-lived B_z northward (positive) excursions marked by vertical blue dashed traces were observed. On the day 08, simultaneous with the CEJ onset (Fig. 7e), there was a short-duration B_z positive excursion from about 14:40 to 15:15 UT with an interleaved southward incursion. Positive B_z excursions, when B_z is in its recovery from negative to positive values, generate overshielding westward electric field E_y (Fejer et al. 1979; Fejer 1986). Kelley et al. (1979) predicted a westward electric field penetration during day when there was a rapid northward excursion of B_z component, which caused the suppression of the equatorial electrojet. Bagiya et al. (2016) also pointed out that during the two-step March 2015 severe magnetic storm, the combined action of the overshielding electric field due to an IMF northward turning and the disturbance dynamo electric field due to the first main phase caused a large TEC depletion over a





large spatial scale. However on day 08, the fast B_z oscillations (north and south) from 14:40 to 15:15 UT canceled out the magnetospheric electric field penetrations and they did not last enough to generate substantial effects. During the storm, we are analyzing the main phase of the first storm began about 21:00 UT on day 07, and during its recovery phase on day 08, a second storm began at about 11:55 UT. These 2 storms were large enough to generate disturbance dynamo (DD) effects, as evidenced by the corresponding large AE values and large negative values of Sym-H (see Fig. 1). Scherliess and Fejer (1997) and Fejer et al. (2005) reported that DD effects are

associated with time delays of about 3–15 h (short term) and 15–24 h (long term) from the storm onset. As DDEF is westward during daytime and evening hours and as large CEJ caused by westward electric field was observed from 14:40 UT up to 15:15 UT on day 08, we suggest that the combination effect of the long-term DDEF from the first storm with the short-term DDEF from the second storm could have caused the CEJ and the downward movement of the *F* region (Fig. 7f) from about 14:40 UT to 16:10 UT. This was followed by inhibition of the prereversal vertical drift and, consequently, to the complete absence of scintillation on the night of day 08.



A penetration of westward electric field to equatorial region, which can inhibit the EIA development, may lead to confinement of the ionospheric plasma to this region with consequent decrease in plasma at low- and middle-latitude sites. During the daytime hours of day 08, large F layer peak density oscillations were observed. Also, a large increase in the F region peak density over São Luís (Fig. 7g) was observed simultaneously with the

F layer height decrease between 14:40 and 16:10 UT, which is in agreement with an EIA weakening caused by a storm-induced westward zonal electric field.

Storm time performance of the new GPS frequencies L2C and L5

To analyze the performance of the new GPS frequencies L2C and L5 during the September 2017 storm, Fig. 8 shows the S4 data from São Luís Septentrio GPS

receiver for the L2C and L5 frequencies. The S4 data from the L1 frequency are also plotted in the figure (in the upper panel). The green line represents the noise threshold, i.e., we consider ionospheric scintillation for $S4 > 0.15$. As the original S4 data were noisy, a Butterworth filter of order 6 was applied. During the storm night 07/08, stronger scintillations were observed as compared to other nights, the L2C scintillations for this night being stronger than at L1, as expected. The scintillations at L5 frequency were as large as that at L1 frequency. However, the number of available GPS satellites from the block IIF, which broadcast the signal at L5 frequency, is actually much smaller (12) than for L1 (31) and L2C (19). For all these 3 GPS frequencies, the scintillation was completely inhibited on the night of 08/09. Weak scintillations were observed again on the night of 10/11.

Latitudinal extension of GPS ionospheric scintillation

To analyze the latitudinal extension of the GPS scintillations during this storm, Fig. 9 shows the S4 parameter during the storm night 07/08 and the second storm recovery phase night 08/09, for some Brazilian GPS

stations from the LISN network which was downloaded from the site <http://lisn.igp.gob.pe>. A Butterworth filter of order 6 was also applied to the original S4 data. From Fig. 9, it can be observed that scintillation was present on the night 07/08 of first storm at all stations, being the S4 peak shifted to later hours as the irregularities are field line mapped from magnetic equator to higher latitudes. Normally, the S4 parameter is larger for stations located under the equatorial ionization anomaly (EIA) crest due to the larger background ionization (de Paula et al. 2003). Since the solar activity was not high enough

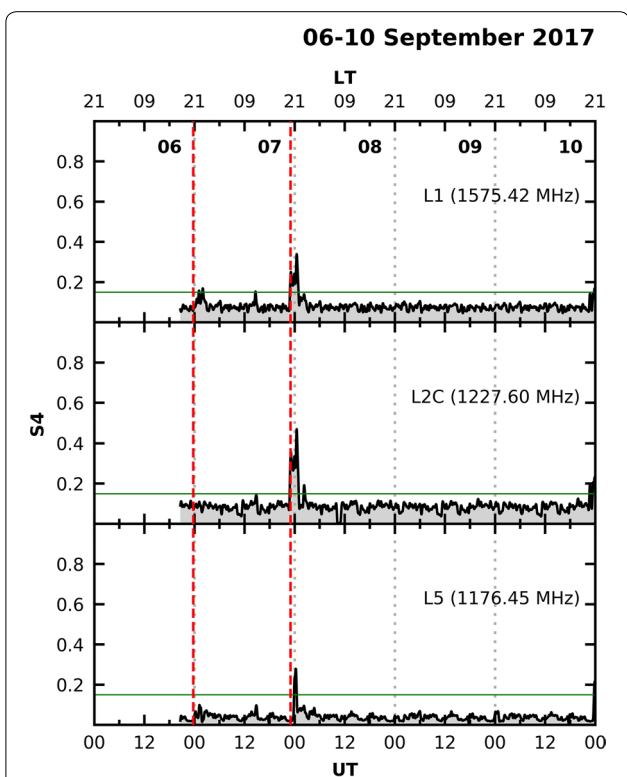


Fig. 8 São Luís PolARx5 GPS receiver S4 parameters for the frequencies L1, L2C and L5 during the storm period. The green line is the noise threshold, i.e., we consider ionospheric scintillation when $S4 > 0.15$. The vertical dashed red lines represent the 2 SSCs, the first one at 23:43 UT on day 06 and the second one 23:00 UT on day 07

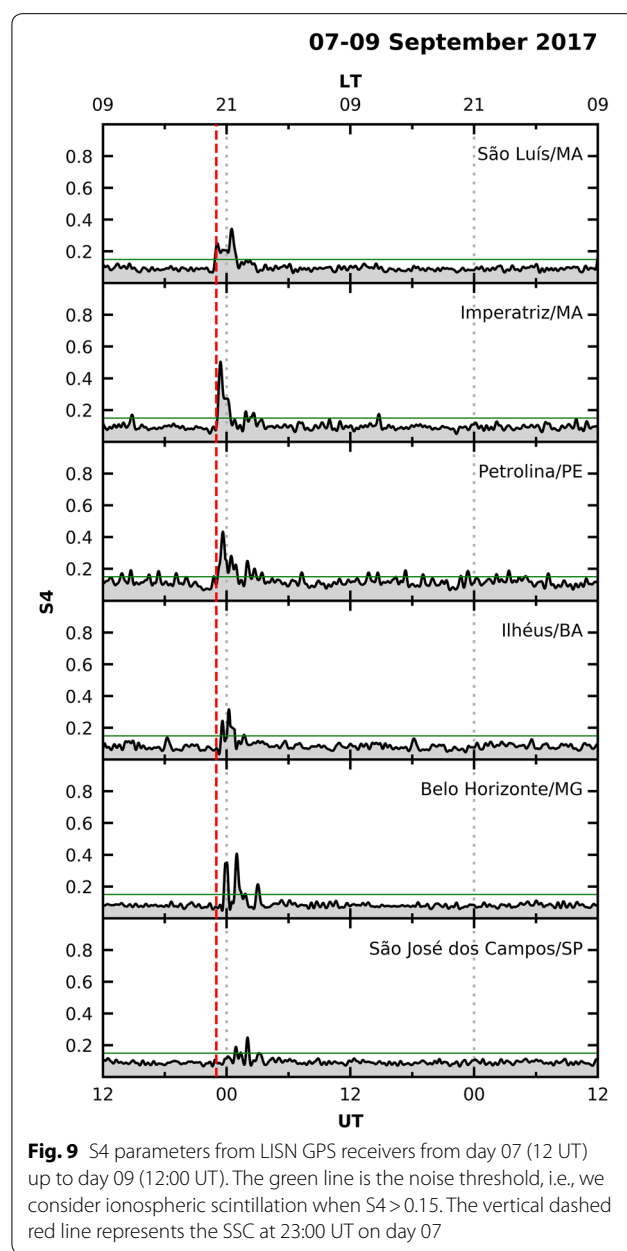


Fig. 9 S4 parameters from LISN GPS receivers from day 07 (12 UT) up to day 09 (12:00 UT). The green line is the noise threshold, i.e., we consider ionospheric scintillation when $S4 > 0.15$. The vertical dashed red line represents the SSC at 23:00 UT on day 07

($F10.7 = 130.4$ s.f.u.) during the day 07, the station of São José dos Campos was outside of the EIA crest with consequently smaller S4 amplitudes. Due to the EIA effect, the S4 values for São Luís, an off equatorial station, are also smaller than the S4 for the other sites located under or closer to the EIA crest. Bhattacharyya et al. (2017) and Kakad et al. (2016) pointed out that at higher altitudes the ESF irregularities have shallower power spectrum due to the presence of small-scale irregularities, which in turn map down to off equatorial stations where ambient electron density is higher, causing stronger L-band scintillations.

Ionospheric irregularity signatures on the SWARM-A electron density

To study the plasma irregularity behavior during this storm, in situ electron density data from the SWARM-A satellite were also analyzed. Figure 10 presents the SWARM-A data in green for the quiet day 03, in red for day 07 including the first storm main phase and recovery initiation and in blue for day 08, during the second storm main phase and part of recovery phase. Figure 10a shows the in situ electron density as a function of geographic latitude, panel b shows the ground projection of the satellite orbits, indicating also the São Luís location (star), and panel c shows the electron density variation as a function of UT ($LT = UT - 03$). These are the selected SWARM-A orbits projection closest to São Luís site around 22 LT (21:30–22:40 LT). As the magnetic declination of São Luís is about $21^\circ W$, and the SWARM-A inclination is almost 90° , the south and north ionospheric regions, where the measurements were made, are not along the same magnetic field line. In Fig. 10a, it can be observed that from 22:15 to 22:40 LT (01:15–01:40 UT) on day 07 (red line) the electron density at 460 km height presented large fluctuations that are signatures of plasma irregularities covering from $45^\circ S$ to $20^\circ N$, compared to the quiet day 03 (green line). Also, large density increase was observed between about $38^\circ S$ and $08^\circ S$ on this day. For the day 08 between about 00:40 and 01:00 UT (21:40–22:00 LT) represented by the blue line, there are no signatures of irregularities. Figure 10c also shows large density fluctuations during day 07 compared to the other 2 days. These results are in agreement with GPS and VHF S4 data as seen in Figs. 3 and 9.

Conclusions

Using the S4 and TEC obtained from GPS and VHF receivers, the data from a Digisonde, and also from the SWARM-A satellite and magnetometers, the ionospheric irregularities over the low-latitude station, São

Luís, were analyzed for the September 06 to 10, 2017 magnetic storm event. S4 parameters from São Luís and from other 5 LISN GPS receivers, as shown in Fig. 2, were also used to study the latitudinal effects of this storm over the ionospheric irregularities. The magnetometer data from a site under the electrojet (Belém) and that from a site outside the effect of the electrojet region effect (Petrolina) were used to infer the daytime vertical plasma drifts. Nighttime plasma drifts were inferred from the São Luís Digisonde during the prereversal hours. The irregularity zonal velocities were measured by VHF receiver using zonally spaced antennas, Digisonde data, and also inferred from GPS TEC data through a keogram analysis. Interplanetary and magnetic data were used to characterize the magnetic storm phases and its association with the above-described parameters. In the period of September 06 to 10, the storm developed in two steps (or 2 storms) associated with the two successive B_z southward incursions with simultaneous AE intensifications, one on day 07

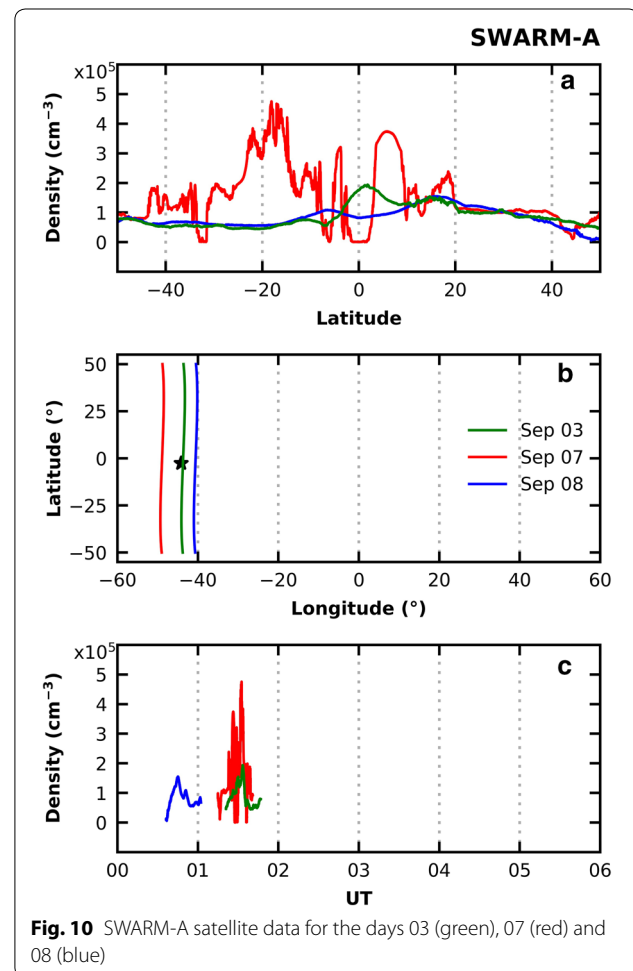


Fig. 10 SWARM-A satellite data for the days 03 (green), 07 (red) and 08 (blue)

and the other on day 08 that occurred in the recovery phase of the first storm.

The main conclusions of this work may be summarized as follows:

- The GPS and VHF amplitude scintillations were observed as S_4 index values that were recorded at 1-min time resolution. The S_4 index was found to increase during hours of evening prereversal vertical drift on the night of 07/08, which was a storm night, in comparison with its quiet time pattern during September 2017. The main phase of the first magnetic storm due to the auroral convection associated with the negative incursion of B_z generated an undershielding eastward electric field that caused a large upward plasma drift during the time of the evening prereversal vertical drift (Fig. 3c), which triggered strong scintillations during the post-sunset hours. Also, the F layer heights measured by the São Luís Digisonde, at the frequencies 3–9 MHz, indicated large peak in the upward prereversal vertical drift for this evening as can be seen in Fig. 6c. Additionally, Fig. 6b shows the occurrence of strong range SF (blue trace) and a short-duration frequency SF on this night, following the $h'F$ upward movement. The $h'F$ values were observed on days 06, 07 and 10 and were relatively large due to the total or partial absorption of the HF wave by the increased D region density produced by the X-ray radiation during this storm;
- The GPS and VHF amplitude scintillations were completely inhibited during the night 08/09. Additionally, SWARM-A satellite electron density measurements did not present signatures of plasma irregularities on this night. The possible cause for the scintillation inhibition is suggested to be the joint effects of the long-term (having time delays of 15–24 h) and short-term (with time delays of 3–15 h) westward DDEF caused by the first and second storm, respectively. This DD westward electric field appears to have caused a strong counter-electrojet (Fig. 7e) as indicated by negative $\Delta H_{\text{Bel-Pet}}$ values, and a downward movement of the F layer height over São Luís (Fig. 7f) during 14:40–15:40 UT. This was followed by total suppression of the prereversal vertical drift on the night of 08/09 and consequently in the inhibition of the scintillation on this night, in agreement with the absence of range and frequency types spread F also on this night. Only a short-duration range SF was observed from 04:30 UT to 06:00 UT on day 09;
- VHF zonal drifts (Fig. 3f) were eastward on the nights of 05/06 (reverting to west around 03:50 UT) and 06/07 (not enough data to reach reversal time), reverted to west on the night 07/08 around 01:44 UT (almost 02 h earlier than on the night 05/06), during the first storm. Abdu et al. (2003) and Santos et al. (2016) pointed out that the thermospheric zonal wind perturbation, as well as the vertical Hall electric field mapped from the E region, could be the drivers for this irregular behavior of the westward drift;
- Zonal plasma irregularity drift obtained from Digisonde and GPS TEC data in the form of a keogram, which are alternative methodologies to infer this parameter, presented a reasonable agreement between themselves during the time interval of 02:00–05:00 UT on the night 07/08, while VHF drift values presented decreasing values along the night. The westward reversal time of the zonal drift on the night 07/08 is around 23:22 UT as inferred by the Digisonde and TEC data, which is more than 2 h earlier than that measured by the VHF system (01:44 UT). The zonal drifts measured by the Digisonde on the storm night 07/08 reversed westward much earlier than on the quiet nights 03/04 and 05/06;
- A comparison of the scintillation among L1, L2C and L5 frequencies (Fig. 8), during the night of 07/08, pointed out that the L2C frequency presented the largest scintillation as to be expected and that L5 scintillations were as large as that at L1, also as expected; however, the number of GPS satellites of the IIF block that transmitted the L5 actually is still small to have a robust and conclusive comparison result;
- The latitudinal extension of scintillation during this storm was analyzed using the GPS data from the different sites covering dip latitudes from 4°S to 21°S. Stronger scintillations triggered by the storm, represented by the S_4 index, were observed during the night 07/08 over all stations, as is noted in Fig. 9. Lower S_4 values were observed over São José dos Campos, located southward of the equatorial ionization anomaly (EIA) crest and São Luís, a low-latitude station. The background ionization is smaller over these two sites for the relatively lower $F_{10.7}$ solar flux level (about 130 s.f.u.) and the correspondingly weaker EIA development. On the night of 08/09, the scintillation was inhibited at all stations, and it occurred again over São Luís (Fig. 8), Imperatriz and Petrolina (not shown) during the night of 09/10;
- Very large electron density fluctuations, which are signatures of plasma irregularities/bubbles, were observed by the SWARM-A satellite at 460 km of altitude (red line in Fig. 9a) in a wide latitudinal range for the first storm day 07 from 22:15 to 22:40 LT, compared to the quiet day 03 (green

line in Fig. 10a). Also, substantial electron density increases were observed from 12°S to 28°S and from 02°N to 10°N on day 07. No signature of plasma irregularities was observed on day 08 from 22:20 to 22:45 LT (blue line of Fig. 8a), which is in agreement with the GPS and VHF ground measurements.

As a final remark, it is important to mention that the ionospheric scintillation measured by the VHF scintillation receiver at São Luís and by many GPS receivers located in a wide latitudinal range from 4.7°S to 20.7°S and longitudinal range of 39°W to 47.4°W had their standard observational data completely modified during the storm of 06 to 10 of September 2017. This modification was in the form of a large scintillation enhancement on the night of 07/08 and a complete scintillation inhibition on the night of 08/09. As the scintillation may affect drastically the VHF/GPS signals and consequently the navigation and positioning systems, as well as some telecommunication systems, it is very important to analyze its behavior during magnetic storms. An important next step following this study is to analyze the effects of such scintillations in the GPS position and navigation results that should permit a deep insight in this field of GPS application.

Authors' contributions

ERP coordinated this study and wrote the first draft of this paper. CBAO generated the keogram related to the TEC data and the vertical and zonal plasma drift components over São Luís inferred by Digisonde data. RGC provided the VHF S4 and zonal drift at São Luís. PMN provided the Digisonde vertical plasma drift using Digisonde data during prereversal hours and using magnetometer data during daytime. ISB reduced and provided Digisonde data for São Luís. ARFM downloaded and analyzed the SWARM-A satellite data and plotted 9 out of 10 figures of the paper. ACN analyzed and provided the São Luís data, and he is responsible for the Digisonde and the AFRL VHF receiver operation at that site. MAA improved substantially to the first draft and provided many scientific ideas during the draft conception. JFGM supervised the TEC analysis and provided ideas for future work. JSS worked together with CBAO in the keogram generation and in the Digisonde data analysis. AOM provided the GPS S4 index for all sites and participated in the scientific discussions that oriented the paper. Besides the above-described contributions, all authors helped to improve the content of this paper. All authors read and approved the final manuscript.

Author details

¹ Instituto Nacional de Pesquisas Espaciais, São José dos Campos, São Paulo 12.227-010, Brazil. ² Instituto Tecnológico de Aeronáutica, São José dos Campos, São Paulo, Brazil. ³ Space Vehicles Directorate, Air Force Research Laboratory, Kirtland AFB, NM 87117, USA. ⁴ Observatório Espacial do Instituto Nacional de Pesquisas Espaciais de São Luís, São Luís, Maranhão 65059-000, Brazil. ⁵ Universidade Estadual Paulista, UNESP, Presidente Prudente, Brazil. ⁶ Instituto de Aeronáutica e Espaço, São José dos Campos, São Paulo, Brazil.

Acknowledgements

Mangalathayil Ali Abdu wishes to thank the Coordenação de Aperfeiçoamento de Pessoal de Nível Superior (Capes) for a senior visiting professorship at ITA/DCTA. E. R. de Paula and J.F.G. Monico acknowledge the support of Conselho Nacional de Desenvolvimento Científico e Tecnológico (CNPq), through Grants 310802/2015-6 and 307417/2017-4, respectively, and INCT GNSS-NavAer Grants 2014/465648/2014-2 CNPq and 2017/01150-0 FAPESP.

A. R. F. Martinon is thankful to FAPESP support under Grant 2017/23220-7. I. S. Batista acknowledges CNPq for support (Grants 302920/2014-5 and 405555/2018-0). C. B. A. de Oliveira is grateful to CNPq 136914/2016-0. A. O. Moraes would like to thank the support of CNPq 314043/2018-7. J. Sousasantos is grateful to FAPESP support under Grant 2018/06158-9. The authors are grateful to Dr. Bela G. Fejer from CASS/USU for the scientific discussions. Monitoring station SLMA (São Luís) was deployed in the context of the Projects CIGALA and CALIBRA, both funded by the European Commission (EC) in the framework of the FP7-GALILEO-2009-GSA and FP7-GALILEO-2011-GSA-1a, respectively, and FAPESP Project Number 06/04008-2.

Competing interests

The authors declare that they have no competing interests.

Availability of data and materials

Digisonde data are available at the site <http://www2.inpe.br/climaespacial/portal/en/>, GPS data at <http://www.ibge.gov.br/home/geociencias/geodesia/rbmc/rbmc.shtml>, magnetometer data at <http://magnetometers.bc.edu/index.php/amber2>, solar flux data at <https://omniweb.gsfc.nasa.gov>, one second and hourly values of V_{sw} , B_z and E_y at <http://omniweb.gsfc.nasa.gov>, SSC data at <http://www.obsebre.es/en/rapid>, SWARM satellite data at <http://earth.esa.int/swarm>, magnetic indices and IGRF at <http://wdc.kugi.kyoto-u.ac.jp/igrf/index.html>, LISN data at <http://lisn.igpp.gob.pe/>, CIGALA/CALIBRA data at <http://is-cigala-calibra.fct.unesp.br/is/>.

Consent for publication

Not applicable.

Ethics approval and consent to participate

Not applicable.

Funding

Not applicable.

Publisher's Note

Springer Nature remains neutral with regard to jurisdictional claims in published maps and institutional affiliations.

Received: 17 December 2018 Accepted: 26 March 2019

Published online: 11 April 2019

References

- Aarons J (1991) The role of the ring current in the generation or inhibition of equatorial F-layer irregularities during magnetic storms. *Radio Sci* 26:1131–1149
- Abdu MA, Kherani EA (2011) Coupling processes in the equatorial spread F/plasma bubble irregularity development. In: Abdu M, Pancheva D (eds) *Aeronomy of the Earth's atmosphere and ionosphere*. IAGA Special Sopron Book Series, vol 2. Springer, Dordrecht, pp 219–238. <https://doi.org/10.1007/978-94-007-0326-1>
- Abdu MA, Batista IS, Takahashi H, MacDougall J, Sobral JHA, Medeiros AF, Trivedi NB (2003) Magnetospheric disturbance induced equatorial plasma bubble development and dynamics: a case study in Brazilian sector. *J Geophys Res* 108(A12):1449. <https://doi.org/10.1029/2002JA009721>
- Abdu MA, de Paula ER, Batista IS, Reinisch BW, Matsuoka MT, Camargo PO, Veliz O, Denardini CM, Sobral JHA, Kherani EA, de Siqueira PM (2008) Abnormal evening vertical plasma drift and effects on ESF and EIA over Brazil–South Atlantic sector during the 30 October 2003 superstorm. *J Geophys Res* 113:A07313. <https://doi.org/10.1029/2007JA012844>
- Abdu MA, Kherani EA, Batista IS, Sobral JHA (2009) Equatorial evening prereversal vertical drift and spread F suppression by disturbance penetration electric fields. *Geophys Res Lett* 36:L19103. <https://doi.org/10.1029/2009GL039919>
- Abdu MA, Nogueira PAB, Santos AM, Souza JR, Batista IS, Sobral JHA (2018) Impact of disturbance electric fields in the evening on prereversal vertical drift and spread F developments in the equatorial ionosphere. *Ann Geophys* 36:609–620. <https://doi.org/10.5194/angeo-36-609-2018>

- Anderson D, Anghel A, Yumoto K, Ishitsuka M, Kudeki E (2002) Estimating daytime vertical E X B drift velocities in the equatorial F-region using ground-based magnetometer observations. *Geophys Res Lett* 29(12):1–4. <https://doi.org/10.1029/2001GL014562>
- Anderson D, Anghel A, Chau J, Veliz O (2004) Daytime vertical E × B drift velocities inferred from ground based magnetometer observations at low latitudes. *Space Weather* 2:S11001. <https://doi.org/10.1029/2004SW000095>
- Bagiya M, Sunda S, Sunil AS (2016) Spatio-temporal dependence effects of the 17 March 2015 space weather event. In: 41st COSPAR scientific assembly, Abstract id. C1.3-10-16, Istanbul, Turkey
- Bhattacharyya A, Basu S, Groves KM, Valladares CE, Sheehan R (2002) Effect of magnetic activity on the dynamics of equatorial F region irregularities. *J Geophys Res* 107:1489. <https://doi.org/10.1029/2002JA009644>
- Bhattacharyya A, Kakad B, Gurram P, Sripathi S, Sunda S (2017) Development of intermediate-scale structure at different altitudes within an equatorial plasma bubble: implications for L-BAND scintillations. *J Geophys Res* 122:1015–1030. <https://doi.org/10.1002/2016JA023478>
- Bittencourt JA, Abdu MA (1981) A theoretical comparison between apparent and real vertical ionization drift velocities in the equatorial F region. *J Geophys Res* 86:2451–2454. <https://doi.org/10.1029/JA086iA04p02451>
- Carter BA, Yizengaw E, Pradipta R, Retterer JM, Groves K, Valladares C, Caton R, Bridgwood C, Norman R, Zhang K (2016) Global equatorial plasma bubble occurrence during the 2015 St. Patrick's day storm. *J Geophys Res* 121:894–905. <https://doi.org/10.1002/2015JA02219>
- de Paula ER, Rodrigues FS, Iyer KN, Kantor IJ, Abdu MA, Kintner PM, Ledvina BM, Kil H (2003) Equatorial anomaly effects on GPS scintillations. *Adv Space Res* 31(3):749–754. [https://doi.org/10.1016/S0273-1177\(03\)00048-6](https://doi.org/10.1016/S0273-1177(03)00048-6)
- de Paula ER, Iyer KN, Hysell DL, Rodrigues FS, Kherani EA, Jardim AC, Rezende LFC, Dutra SG, Trivedi NB (2004) Multi-technique investigations of storm-time ionospheric irregularities over the São Luís equatorial station in Brazil. *Ann Geophys* 22:3513–3522. <https://doi.org/10.5194/angeo-22-3513-2004>
- de Paula ER, Kherani EA, Abdu MA, Batista IS, Sobral JHA, Kantor IJ, Takahashi H, Rezende LFC, Muella MTAH, Rodrigues FS, Kintner PM, Ledvina BM, Mitchell C, Groves KM (2007) Characteristics of the ionospheric irregularities over Brazilian longitudinal sector. *Indian J Radio Space Phys* 36:268–277
- de Paula ER, Jonah OF, Moraes AO, Kherani EA, Fejer BG, Abdu MA, Muella MTAH, Batista IS, Dutra SLG, Paes RR (2015) Low-latitude scintillation weakening during sudden stratospheric warming events. *J Geophys Res Space Phys*. <https://doi.org/10.1002/2014JA020731>
- Engavale B, Jeeva K, Nair KU, Bhattacharyya A (2005) Solar flux dependence of coherence scales in scintillation patterns produced by ESF Irregularities. *Ann Geophys*. <https://doi.org/10.5194/angeo-23-3261>
- Fejer BG (1986) Equatorial ionospheric electric fields associated with magnetospheric disturbances. In: Kamide Y, Slavin JA (eds) *Solar wind magnetosphere coupling*. Terra Sci., Tokyo, pp 519–545
- Fejer BG, Scherliess L (1997) Empirical models of storm time equatorial zonal electric fields. *J Geophys Res* 102:24047–24056
- Fejer BG, Gonzales CA, Farley DT, Kelley MC, Woodman RF (1979) Equatorial electric fields during magnetically disturbed conditions: 1. The effect of the interplanetary magnetic field. *J Geophys Res* 84:5797–5802. <https://doi.org/10.1029/JA084iA10p05797>
- Fejer BG, Scherliess L, de Paula ER (1999) Effects of the vertical plasma drifts velocity on the generation and evolution of equatorial spread F. *J Geophys Res* 104:19859–19869. <https://doi.org/10.1029/1999JA000271>
- Fejer BG, Souza JR, Santos AS, Costa Pereira AE (2005) Climatology of F region zonal plasma drifts over Jicamarca. *J Geophys Res* 110:A12310. <https://doi.org/10.1029/2005JA011324>
- Groves KM, Basu S, Weber EJ, Smitham M, Kuenzler H, Valladares CE, Sheehan R, MacKenzie E, Secan JA, Ning P, McNeil WJ, Moonan DW, Kendra MJ (1997) Equatorial scintillation and systems support. *Radio Sci* 32:2047
- Huang C-S, Roddy PA (2016) Effects of solar and geomagnetic activities on the zonal drift of equatorial plasma bubbles. *J Geophys Res* 121:628–637. <https://doi.org/10.1002/2015JA021900>
- Kakad B, Nayak CK, Bhattacharyya A (2012) Power spectral characteristics of ESF irregularities during magnetically quiet and disturbed days. *J Atmos Sol Terr Phys* 81:41–42. <https://doi.org/10.1029/2006JA01202>
- Kakad B, Gurram P, Tripura Sundari PNB, Bhattacharyya A (2016) Structuring of intermediate scale equatorial spread F irregularities during intense geomagnetic storm of solar cycle 24. *J Geophys Res* 121(7):7001–7012. <https://doi.org/10.1002/2016ja022635>
- Kakad B, Surve G, Tiwari P, Yadav V, Bhattacharyya A (2017) Disturbance dynamo effects over low latitude F-region: a study by network of VHF spaced receivers: disturbed time zonal plasma drifts. *J Geophys Res*. <https://doi.org/10.1002/2016ja023498>
- Kelley MC, Fejer BG, Gonzales CA (1979) An explanation for anomalous equatorial ionospheric electric fields associated with a northward turning of the interplanetary magnetic field. *Geophys Res Lett* 6(4):301–304. <https://doi.org/10.1029/GL006i004p00301>
- Keskinen MJ, Ossakow SL, Fejer BG (2003) Three-dimensional nonlinear evolution of equatorial spread-F bubbles. *Geophys Res Lett* 30(16):1855. <https://doi.org/10.1029/2003GL017418>
- Li G, Ning B, Zhao B, Liu L, Liu JY, Yumoto K (2008) Effects of geomagnetic storm on GPS ionospheric scintillations at Sanya. *J Atmos Solar Terr Phys* 70:1034–1045. <https://doi.org/10.1016/j.jastp.2008.01.003>
- Martinis CR, Mendillo MJ, Aarons J (2005) Toward a synthesis of equatorial spread F onset and suppression during geomagnetic storms. *J Geophys Res* 110:A07306. <https://doi.org/10.1029/2003JA0101362>
- Muella MTAH, Duarte-Silva MH, Moraes AO, de Paula ER, Rezende LFC, Alfonsi L, Affonso BJ (2017) Climatology and modeling of ionospheric scintillations and irregularity zonal drifts at the equatorial anomaly crest region. *Ann Geophys* 35:1201–1218. <https://doi.org/10.5194/angeo-35-1201-2017>
- Nayak C, Tsai L-C, Su S-Y, Galkin IA, Caton RG, Groves KM (2017) Suppression of ionospheric scintillation during St. Patrick's Day geomagnetic super storm as observed over the anomaly crest region station Pingtung, Taiwan: a case study. *Adv Space Res* 60:396–405. <https://doi.org/10.1016/j.asr.2016.11.036>
- Reinisch BW, Scali JL, Haines DM (1998) Ionospheric drift measurements with ionosondes. *Ann di Geofis* 41:695–702
- Santos AM, Abdu MA, Souza JR, Sobral JHA, Batista IS, Denardini CM (2016) Storm time equatorial plasma bubble zonal drift reversal due to disturbance Hall electric field over the Brazilian region. *J Geophys Res Space Phys* 121:5594–5612. <https://doi.org/10.1002/2015JA022179>
- Scherliess L, Fejer BG (1997) Storm time dependence of equatorial disturbance dynamo zonal electric fields. *J Geophys Res* 102:24037–24046. <https://doi.org/10.1029/97JA02165>
- Sultan PJ (1996) Linear theory and modeling of the Rayleigh–Taylor instability leading to the occurrence of equatorial spread F. *J Geophys Res* 101:26875–26891. <https://doi.org/10.1029/96JA00682>